Title

Comparing measurement of limiting current in block copolymer electrolytes as a function of salt concentration with theoretical predictions

Authors

Frenck, Louise
Veeraraghavan, Vijay D
Maslyn, Jacqueline A
et al.

Publication Date

2022-03-01

DOI

10.1016/j.electacta.2022.139911

Comparing Measurement of Limiting Current in Block Copolymer Electrolytes as a Function of Salt Concentration with Theoretical Predictions

Louise Frenck[a,b], Vijay D. Veeraraghavan[a], Jacqueline A. Maslyn[a,b] Nitash P. Balsara[a,b]

[a]Department of Chemical and Biomolecular Engineering, University of California, Berkeley, California 94720, United States

[b]Materials Sciences Division, Lawrence Berkeley National Laboratory, Berkeley, California 94720, United States

KEYWORDS: "Lithium", "Polymer Electrolyte", "Salt Concentration Gradient", "Concentrated Solution Theory", "Limiting current density".

ABSTRACT

Optimizing electrolyte performance is crucial for the widespread adoption of electrochemical energy storage. We demonstrate that limiting current provides a robust criterion for determining the optimum electrolyte. Experiments were conducted on rigid block copolymer electrolytes comprising mixtures of polystyrene-*block*-poly(ethylene oxide) copolymer (SEO) and lithium bis(trifluoromethanesulfonyl) imide salt (LiTFSI) over a salt concentration range from r_{av} = 0.04 to r_{av} = 0.20 (r_{av} is the molar ratio of lithium ions to ethylene oxide). We show that the maximum limiting current density is 4.3 mA cm^{-2} at r_{av} = 0.12. The dependence of limiting current on salt concentration is in good agreement with predictions from Newman's concentrated solution theory with no adjustable parameters.

1. INTRODUCTION

The need to develop new rechargeable battery chemistries is well-established.[1,2] One approach for increasing the energy density of lithium batteries is by replacing the graphite battery anode with lithium metal.[3,4] Commercial lithium metal batteries are limited, and one of the problems associated with these batteries is the formation of dendrites on the lithium metal negative electrode during charging.[5–7] Block-copolymer electrolytes with a rigid non-conducting domains and a flexible ion conducting domains are potential candidates to solve this problem.[8] The rigid domains are designed to prevent dendrite formation, while the flexible domains provide avenues for ion transport between the electrodes.

The limiting current density is one parameter that determines whether or not a given electrolyte can be used in an application. The limiting current is defined as the steady current at which the lithium ion concentration at the cathode approaches zero.[9–12] The continuous application of current induces concentration polarization in the electrolyte and the limiting current density signifies the maximum concentration polarization that can be accommodated in an electrolyte.[13–16] Exceeding the limiting current density will lead to degradation of the electrolyte in the vicinity of the cathode. Despite the clearly established importance of the limiting current density in the literature, this parameter is very rarely measured.[17–21]

The symmetric lithium-electrolyte-lithium cell is a convenient platform for defining the limiting current density (as opposed to cells including a composite electrode comprising a large number of particles) because the locations of the planar electrodes are well defined. It is, however, not trivial to measure limiting current density if issues related to dendrite formation have not been resolved. It is clear that the introduction of non-planar structures, such as

dendrites, will interfere with limiting current density measurements. Block copolymer electrolytes wherein dendrite formation is suppressed are thus ideally suited for measuring limiting current density.[22]

We report herein on electrolytes comprising mixtures of polystyrene-*block*-poly(ethylene oxide) (PS-*b*-PEO, or SEO) copolymer with lithium bis(trifluoromethanesulfonyl)imide salt (LiTFSI). Our work covers a broad range of salt concentration from r_{av} = 0.04 to 0.20, where r_{av} is the molar ration of lithium ions to ethylene oxide monomer units. Ion transport on the continuum scale can be rigorously predicted by Newman's concentrated solution theory: [23–26] this requires measurements of three transport parameters (conductivity, κ, salt diffusivity, D, and the cation transference number in respect to the solvent velocity, t_+^0) and the thermodynamic factor. These parameters have been measured for the electrolytes used in this study and can be found in ref [27]. We can thus predict the dependence of limiting current density on salt concentration. In addition, we can predict the potential drop versus current characteristic of our electrolytes at currents below the limiting current density. We present comparison between experiments and theory with no adjustable parameters. We demonstrate the existence of an optimal electrolyte that maximizes the limiting current density.

2. METHODS

2.1. Materials

In this study we use a polystyrene-*b*-polyethylene oxide diblock copolymer (PS-PEO or SEO), which was synthesized by anionic polarization polymerization as described in previous work. [28–30] The molecular weight of the two blocks were $M_{w(PS)}$= 235 kg mol^{-1} and $M_{w(PEO)}$ = 222 kg mol^{-1} for PS and PEO respectively. The polydispersity index in N-methyl-2-pyrrolidone (NMP) with respect to a polystyrene standard, PDI is 1.05. Lithium

bis(trifluoromethanesulfonyl) imide salt (LiTFSI) is added to the polymer in order to obtain a conductive electrolyte, the molar ratio r_{av} is defined as the molar ratio of lithium ions to the ethylene oxide moieties.[31] We studied a wide salt concentration range of electrolytes with r_{av} = 0.04, 0.06, 0.085, 0.10, 0.12, 0.15, 0.18, 0.20. An argon filled glovebox with less than 1 ppm of water and less than 1 ppm of oxygen was used to prepare all electrolytes and all electrochemical cell assembly steps were performed in it to avoid any contamination.

2.2. Electrolyte casting and lithium-lithium symmetric cell assembling

Electrolyte casting methods, as well as lithium-lithium symmetric cells assembly methods, closely mimic those previously reported.[32–35] The solvent used to cast membrane was NMP. This method results in freestanding electrolyte films of about 50µm thickness. Lithium metal foil used in this study was purchased from FMC Lithium at 99.9% purity (thickness of 150 µm). All cells were vacuum sealed inside a polypropylene-lined aluminum pouch material (Showa-Denko) in order to perform our experiments outside the glovebox.

2.3. Limiting current density experiment

Limiting current density experiments were inspired by methods reported in Hudson[21] and Maslyn et al.[22]. Lithium-lithium (Li-Li) symmetric cells were first annealed at 120ºC for 4h in order to erase the electrolyte temperature history. Then cells were allowed to equilibrate at 90 ºC for one hour before performing the experiments. All experiments were performed at 90ºC. The Li-Li symmetric cells were first conditioned at a low current density of i = 0.02 mA cm^{-2} for 15 cycles, using a BioLogic VMP3 potentiostat, in order to ensure a stable interface between the polymer electrolyte and lithium electrodes. One cycle consisted in 4h positive polarization followed by 45 min of rest, then 4h negative polarization followed by 45min of rest. In order to determine the limiting current, a series of alternative positive and negative polarizations were run

onto the cells. First, Li-Li symmetric cells were run at 3 low current densities (i = 0.05, 0.08, 0.1 mA cm^{-2}) for 15 min each, followed by 30 min of rest to allow for relaxation, in order to sample the linear regime for the current-voltage relationship. As soon as a steady-state potential was reached during polarization, the applied current was stopped in order to minimize formation of lithium protrusions which can short circuit the cell prematurely. After observing the linear regime at three low current densities, cells were run at high current density to see the divergence of the potential, which is the signature of limiting current density exceeded. Next, the applied current density was decreased incrementally until a steady state voltage was again observed in response to the applied constant current. After each polarization, cells were let to rest for 30 min or until complete relaxation of the potential. After each polarization and rest steps, electrochemical impedance spectroscopy measurements were run, for a frequency range from 1 MHz to 1 Hz at an amplitude of 40mV, to confirm that the cell was not damaged.

3. RESULTS AND DISCUSSION

Figure 1

Figure 1 shows the typical potential drop over the electrolyte versus time data obtained at different current densities for one electrolyte (r_{av} = 0.085). Each curve represents the time dependence of the normalized potential drop over the electrolyte $|\Phi|L^{-1}$, where Φ is the measured voltage response corrected for the potential drop due to interfacial impedance and L is the electrolyte thickness, at fixed applied current density, i. Our approach for determining Φ is given in ref [23] and [22]. The potential drop accounting for the drop due to the interfaces is calculated using $\Phi = \Phi_{,\text{measured}} - iR_iA$, where Φ_{measured} is the measured potential drop, R_i is the interfacial resistance measured by impedance spectroscopy after each polarization, and A is the cell area.

We begin with small applied current densities (i = 0.08 mA cm^{-2} and below) to ensure that the cell has been properly assembled and conditioned. We then step up the current and obtain potential versus time curves that either saturate or diverge at long times (0.55 ≤ i ≤ 1.50 mA cm^{-2}). Saturation behavior is seen at all current densities i < 1.0 mA cm^{-2}. The upper limit of this range is labelled "largest sustainable current density" in Figure 1. Divergent behavior, which is a signature that the lithium ion concentration at the cathode approaches zero and that the reductive redox reaction is compromised,[25] is seen at current densities greater than i = 1.35 mA cm^{-2}. Beyond the limiting current density, the electrons in the negative electrode cannot react with lithium ions and therefore are forced to participate in irreversible reactions with the polymer. The unstable potential versus time response seen at i ≥ 1.35 mA cm^{-2} in Figure 1 is a signature of these irreversible redox reactions. The lower limit of this range is labelled "smallest unsustainable current density" in Figure 1. In the example in Figure 1, the highest sustainable current density is found to be i = 1.00 mA cm^{-2}, while the smallest unsustainable current density is found to be i = 1.35 mA.cm^{-2}. Therefore, we define the experimental limiting current, i_L, as the average between the highest sustainable measured current density and the smallest unsustainable measured current density, here i_L = 1.175 mA cm^{-2}. These steps were reproduced for each salt concentration studied.

Figure 2

This procedure was repeated for 4 to 6 cells for several salt concentrations. Figure 2 shows the results of these experiments. The measured data are presented using the right y-axis where the product $i_L L$ is plotted as a function of r_{av}. This format accounts for unavoidable differences in electrolyte thickness from cell to cell. On the left y-axis, the limiting current density is normalized to a thickness of 20 μm, $i_{Lnorm,}$ assuming that the product $i_L L$ is a constant

as predicted by Eq 1. We used 20 µm as it is the thickness of standard separators used in Li-ion batteries: [36]

$$i_{\mathrm{L,norm}} = i_{L,exp}\frac{L}{20}, \qquad \text{Eq. 1}$$

where $i_{L,exp}$ is the experimentally determined limiting current density (mA cm^{-2}) and L the measured thickness of the electrolyte (µm).

At low r_{av} values, the limiting current density increases almost linearly from i_{Lnorm} = 0.94 mA cm^{-2} for r_{av} = 0.04, up to i_{Lnorm} = 4.3 mA cm^{-2} for r_{av} = 0.12. At r_{av} values higher than r_{av} = 0.12, the limiting current density decreases from i_{Lnorm} = 4.3 mA cm^{-2} for r_{av} = 0.12 to i_{Lnorm} = 3.3 mA cm^{-2} for r_{av} = 0.20.

Newman derived a simple expression for the limiting current density in a dilute electrolyte,[37]

$$i_L = \frac{2cDF}{L(1-\rho_+)}, \qquad \text{Eq. 2}$$

where c is the molar salt concentration (mol cm^{-3}), D is the salt diffusion coefficient (cm^2 s^{-1}), F is the Faraday constant (C mol^{-1}), L is the thickness of the electrolyte (20µm). In dilute electrolytes the cation transference number can be approximated by ρ_+, the current fraction measured by methods proposed by Watanabe, Bruce, Vincent, and coworkers' methods.[13,38] We used the same formulas for our block copolymer electrolyte assuming that c is the molar concentration of the salt in the ionic conducting domains, the parameters D and ρ_+ for our electrolyte are given in ref [27] and reproduced in the SI Figure S1. The limiting current density calculated using Eq 2 is shown in Figure 2 as a dashed line. One generally expects the limiting current density to increase with increasing salt concentration. The experimental observation of a

regime where the limiting current density decreases with increasing salt concentration is therefore unexpected.

It is clear from Figure 2 that dilute solution theory cannot fully account for the experimental results. We therefore use Newman's concentrated solution theory[26] to obtain a more rigorous prediction of limiting current density. We use the approach developed by Pesko et al.[25] and Frenck et al.[27] wherein the concentration gradient as a function of position is calculated using Equation 2.

$$\int_{r(x=0)}^{r(x)} \frac{D(r)c(r)}{r_{av}t_{-}^{0}(r)}dr = \int_{r(x=0)}^{r(x)} \frac{\kappa(r)}{\left(1-\frac{1}{\rho_{+}(r)}\right)(z_{+}\nu_{+})r_{av}F\varphi_{c}(r)}\left(\frac{dU}{dlnm}\right)dr = \int_{r(x=0)}^{r(x)} J(r)\,dr = -\frac{i\,L}{F}\left(\frac{x}{L}\right), \quad \text{Eq. 3}$$

where κ is the ionic conductivity (S cm^{-1}), φ_c is the volume fraction of the conducting phase, z_+ is the charge number of the cation, ν_+ is the number of cations in the dissociated salt, U is the open circuit potential, m is the molality of salt in the conducting phase, and $\frac{dU}{dlnm}$ is the change in the open potential. The dependence of κ, φ_c, c, U and m on r is given in ref [27] and [39] and reproduced in the SI.

The potential drop, Φ, at steady state can be predicted using the Equation 3,

$$\Phi(x) = F\int_{r(x=L)}^{r(x)} \frac{D(r)c(r)}{r_{av}t_{-}^{0}(r)\kappa(r)\rho_{+}(r)}dr\,, \quad \text{Eq.4}$$

where, t_{-}^{0} is the anion transference number with respect to the solvent velocity, t_{-}^{0} = 1 - t_{+}^{0}.

Furthermore, substituting $J(r)$ in equation 4, we can rewrite equation 4 as a function of measured parameters as shown in Eq.5:

$$\Phi(x) = F\int_{r(x=L)}^{r(x)} \frac{1}{(\rho_{+}(r)-1)(z_{+}\nu_{+})r_{av}F\varphi_{c}(r)}\left(\frac{dU}{dlnm}\right)dr = F\int_{r(x=L)}^{r(x)} G(r)\,dr, \quad \text{Eq. 5}$$

Figure 3

Figure 3 presents the calculated concentration dependent functions $J(r)$ and $G(r)$ as a function of salt concentration using equations 3 and 5. A polynomial fit and a double exponential fit of the functional form given in equation 6 and equation 7, respectively, were used in each case in order to calculate the corresponding integrals. Fits are shown as dashed curves in both Figure 3(a) and Figure 3(b).

$$J(r_{av}) = ar_{av}^6 + br_{av}^5 + cr_{av}^4 + dr_{av}^3 + er_{av}^2 + fr_{av} + g, \quad \text{Eq. 6}$$

$$G(r_{av}) = k_0 + A_1 \exp(-\tau_1 r_{av}) + A_2 \exp(-\tau_2 r_{av}), \quad \text{Eq. 7}$$

Table 1 gives the fitting parameters for $J(r)$ and $G(r)$.

$J(r_{av})$	a	b	c	d	e	f	g
	-3.98×10^{-4}	3.80×10^{-4}	-1.46×10^{-4}	2.88×10^{-5}	-3.03×10^{-6}	1.55×10^{-7}	-2.52×10^{-9}
$G(r_{av})$	k_0	A_1	A_2	τ_1	τ_2		
	1.12×10^{-5}	2.06×10^{-5}	2.38×10^{-5}	8.22	8.56		

Table 1. Fitting parameters for $J(r_{av})$ and $G(r_{av})$ used to obtain the polynomial and double exponential fits showed as dashed curved in Figure 3(a) and 3(b) respectively.

By integrating Equation 3 between $r(x = 0)$ and $r(x)$, we can model the salt concentration profile, r, at a given r_{av} and a given current density, i. This procedure is repeated with increasing values of i until the concentration at the cathode ($x/L = 1$) reaches zero, which corresponds to the limiting current density. Figure 4(a) presents an example of salt concentration profiles as a function of position in the cell ($0 \leq x/L \leq 1$) calculated using Eq.3 for a cell with an electrolyte of $r_{av} = 0.085$ at different current densities, from $i = 0.20$ mA cm^{-2} to $i = 2.80$ mA cm^{-2}. The colormap indicates the current density for each salt concentration profile. We see an increase in the salt concentration gradient as i is increased. The limiting current density is

reached for this particular electrolyte at i = 2.80 mA cm^{-2} (pink curve). This theoretical limiting current density, $i_{L,theo}$, was determined for each salt concentration using the same procedure.

Figure 4

Figure 4b shows the calculated spatially dependent steady-state potential normalized by cell thickness, $\Phi_{SS}\, L^{-1}$, as a function of current density and position in the cell x/L using Eq 5. The value of $\Phi_{SS}\, L^{-1}$ at x/L= 0 represents the average potential gradient across the electrolyte at the specified current density. As i is increased, the steady-state potential profile increases, as expected.

Figure 5

Figure 5 compares the experimentally measured $\Phi_f L^{-1}$ (markers) with theoretical predictions for $\Phi_{SS}\, L^{-1}$ (dashed curve) as a function of r_{av}, for three current densities: i = 0.02, 0.05 and 0.08 mA cm^{-2}. We choose these current densities as they are below the limiting current density of all electrolytes covered in this study. We can see that the measured $\Phi_f\, L^{-1}$ is a complex function of salt concentration. The qualitative features of the dependence of $\Phi_f\, L^{-1}$ on r_{av} is similar at all three current densities. At i = 0.02 mA cm^{-2}, we find two local minima at r_{av}= 0.06 and r_{av} = 0.18, with a local maximum at an intermediate value at r_{av} = 0.12. The local minimum at low salt concentration is in quantitative agreement with theoretical predictions. The theoretical maximum is predicted at r_{av} = 0.18 which is somewhat higher than the experimental value. Similar agreement between theory and experiments is obtained at i = 0.05 and 0.08 mA cm^{-2}. It is clear from Figure 5 that predictions based on concentrated solution theory capture the complex dependence of $\Phi_f\, L^{-1}$ on r_{av}. This is remarkable because concentrated solution theory[26] was not originally developed for predicting the potential versus current characteristics of nanostructured materials.[22,39] For battery applications the optimal salt concentration would be

to the case where $\Phi_f L^{-1}$ is minimized; therefore the local minima in Figure 5 are of practical significance.

Figure 6

We now return to the experimentally measured limiting current density as a function of salt concentration and compare these results with theoretical predictions. Figure 6 shows the experimentally measured limiting current densities normalized to a 20 µm thick electrolyte, $i_{L,norm}$, while the theoretical calculated limiting current density, $i_{L,theo}$, is shown as a blue solid line. The right y-axis shows the limiting current density multiplied by the cell thickness, $i_L L$. In our theoretical predictions, we see an increase in the limiting current density as the salt concentration increases, until it reaches a maximum, $i_{L,max}$, for r_{av} = 0.15 with $i_{L,max}$ = 5.85 mA cm^{-2}. The same general behavior is seen experimentally. The experimentally determined value of $i_{L,max}$ is 4.30 mA cm^{-2} and it is obtained at r_{av} = 0.12. Note that the experimental data in Figure 5 indicates that the least efficacious electrolyte is one with r_{av} = 0.12. In contrast, the limiting current density analysis indicates that the optimal electrolyte is the one with r_{av} = 0.12. This difference arises because the data in Figure 5 were obtained at low current densities, while the optimum in Figure 6 reflects electrolyte properties at high current densities. The optimal limiting current of SEO/LITFSI electrolytes is well below that of PEO/LiTFSI electrolytes, wherein i_L = 20.8 mA cm^{-2} for a 20 µm thick electrolyte was obtained for r_{av} = 0.085.

4. CONCLUSION

Optimizing battery performance is crucial for the widespread adoption of electrical energy storage. The electrolyte is a key component as it transports the working ion between the positive and negative electrodes. Conductivity is often used as the criterion for determining the

optimum electrolyte. This transport parameter is of limited value as it reflects the motion of both the cation and the anion, and it does not reflect the nature of salt concentration gradients that occur under dc polarization. In this paper we demonstrate that limiting current provides a robust criterion for determining the optimum electrolyte. If the concentration dependence of transport parameters is ignored, limiting current is a monotonically increasing function of salt concentration.[37] If this is true, the optimal electrolyte is one with the highest salt concentration.

Experiments were conducted on rigid block-copolymer electrolytes composed of mixtures of an SEO block copolymer and LiTFSI with a salt concentration range from r_{av} = 0.04 to r_{av} = 0.20. These experiments extend our previous work on limiting current and block copolymer electrolytes which examine SEO LiTFSI mixtures at three r_{av} values, from r_{av} = 0.04, 0.085 and 0.12.[22] In addition, the more complete present study shows that the limiting current density, $i_{L,}$ increases with increasing salt concentration until reaching a maximum of 4.3 mA cm^{-2} at r_{av} = 0.12. At higher concentrations, i_L decreases with increasing salt concentration. The optimal SEO/LiTFSI electrolyte is thus one with r_{av} = 0.12. The stability of block copolymer electrolytes against lithium metal anodes and dendrites prevention is the subject of a number of previous publications[32,34,40–44]. Our ability to measure limiting current at high salt concentrations is entirely due to this stability. In homopolymer PEO electrolyte for example, we could not measure limiting current above r_{av} = 0.085 due to rapid growth of lithium dendrites

We used Newman's concentrated solution theory to predict the limiting current density. We also use this theory to predict the potential needed to drive current through the SEO/LiTFSI electrolytes as a function of current density (below the limiting current) and salt concentration. At low current densities, the dependence of potential on salt concentration is complex; we obtain

two local minima separated by a maximum at r_{av} = 0.12. This observation would suggest that the SEO/LiTFSI electrolyte with r_{av} = 0.12 is suboptimal. It is clear that analysis at low current densities may not accurately reflect electrolyte behavior in the vicinity of the limiting current.

5. ABREVIATION AND SYMBOL

Symbol	
$\boldsymbol{c}$	Concentration of lithium salt in the conducting phase [mol cm^{-3}]
$\boldsymbol{D}$	Salt diffusion coefficient [cm^2 s^{-1}]
$\frac{\boldsymbol{dU}}{\boldsymbol{dlnm}}$	Change in open-circuit potential with respect to the logarithm of the molal concentration of salt in the electrolyte [V]
$\boldsymbol{F}$	The Faraday constant [C mol^{-1}]
$\boldsymbol{i}$	Current density [mA cm^{-2}]
$\boldsymbol{i_{L,exp}}$	Experimentally measured limiting current density [mA cm^{-2}]
$\boldsymbol{i_{L,max}}$	Predicted maximum limiting current density using Newman's concentrated solution theory [mA cm^{-2}]
$\boldsymbol{i_{L,norm}}$	Normalized limiting current density [mA cm^{-2}]
$\boldsymbol{i_L}$	Limiting current density [mA cm^{-2}]
$\boldsymbol{r_{av}}$	Salt concentration in the PEO-rich phase, defined as the molar ratio, $\frac{\mathbf{[LiTFSI]}}{\mathbf{[EO]}}$
$\boldsymbol{\kappa}$	Ionic conductivity measured in a cell with blocking electrodes [S cm^{-1}]
$\boldsymbol{t_-^0}$	Concentrated solution theory transference number of the anion with respect to the solvent velocity; $\boldsymbol{t_-^0 = 1 - t_+^0}$
$\boldsymbol{z_+}$	Charge number of the cation
$\boldsymbol{\rho_+}$	Current fraction

$\boldsymbol{v_+}$	Number of cations in the dissociated salt
$\boldsymbol{\varphi_c}$	Volume fraction of the conducting phase
$\boldsymbol{L}$	Electrolyte thickness [cm]
Li	Lithium
LiTFSI	Lithium bis(trifluoromethanesulfonyl) imide salt
$\mathbf{M_{w(PEO)}}$	Molecular weight of the poly(ethylene oxide) block
$\mathbf{M_{w(PS)}}$	Molecular weight of the poly(styrene) block [kg mol^{-1}]
NMP	N-methyl-2-pyrrolidone
PEO	Poly(ethylene oxide)
PS	Poly(styrene)
PS-*b*-PEO SEO	Poly(ethylene oxide)-*block*-Poly(styrene) copolymer
$\boldsymbol{\Phi}$	Measured potential corrected for the potential drop due to interfacial impedance [V]
$\boldsymbol{\Phi_f}$	Experimentally measured steady-state electric potential [V]
$\boldsymbol{\Phi_{SS}}$	Steady-state electric potential [V]
$\boldsymbol{r}$	Salt concentration profile
$\boldsymbol{r_{av}}$	Salt concentration in the PEO-rich phase, defined as the molar ratio, $\frac{\mathbf{[LiTFSI]}}{\mathbf{[EO]}}$
$\boldsymbol{V}$	Voltage [V]
$\boldsymbol{x}$	Position in the electrolyte [cm]

ASSOCIATED CONTENT

The following file is available free of charge.

Supplementary Information (PDF)

AUTHOR INFORMATION

Corresponding Author

* E-mail: nbalsara@berkeley.edu. Phone: 1-510-642-8973

* Address: 201C Gilman Hall, Berkeley, CA 94720

ORCID

Louise Frenck: 0000-0001-7116-2144
Vijay D. Veeraraghavan: 0000-0001-7327-7316
Jacqueline A. Maslyn: 0000-0002-6481-2070
Nitash P. Balsara: 0000-0002-0106-5565

Author Contributions

J.A.M. synthesized SEO block copolymer. L.F. and V.V fabricated samples and performed the experiments. L.F. and N.P.B. prepared figures and composed the manuscript. N.P.B. directed the work.

Notes

The authors declare no competing financial interest.

ACKNOWLEDGMENT

This work was supported by the Assistant Secretary for Energy Efficiency and Renewable Energy, Office of Vehicle Technologies of the U.S. Department of Energy under Contract DE-AC02-05CH11231 under the Battery Materials Research Program.

REFERENCES

[1] L. Trahey, F.R. Brushett, N.P. Balsara, G. Ceder, L. Cheng, Y.-M. Chiang, N.T. Hahn, B.J. Ingram, S.D. Minteer, J.S. Moore, K.T. Mueller, L.F. Nazar, K.A. Persson, D.J. Siegel, K. Xu, K.R. Zavadil, V. Srinivasan, G.W. Crabtree, Energy storage emerging: A perspective from the Joint Center for Energy Storage Research, PNAS. 117 (2020) 12550–12557. https://doi.org/10.1073/pnas.1821672117.

[2] M. Armand, P. Axmann, D. Bresser, M. Copley, K. Edström, C. Ekberg, D. Guyomard, B. Lestriez, P. Novák, M. Petranikova, W. Porcher, S. Trabesinger, M. Wohlfahrt-Mehrens, H. Zhang, Lithium-ion batteries – Current state of the art and anticipated developments, Journal of Power Sources. 479 (2020) 228708. https://doi.org/10.1016/j.jpowsour.2020.228708.

[3] D. Aurbach, Review of selected electrode–solution interactions which determine the performance of Li and Li ion batteries, Journal of Power Sources. 89 (2000) 206–218. https://doi.org/10.1016/S0378-7753(00)00431-6.

[4] M.S. Whittingham, Special Editorial Perspective: Beyond Li-Ion Battery Chemistry, Chem. Rev. 120 (2020) 6328–6330. https://doi.org/10.1021/acs.chemrev.0c00438.

[5] D. Aurbach, E. Zinigrad, Y. Cohen, H. Teller, A short review of failure mechanisms of lithium metal and lithiated graphite anodes in liquid electrolyte solutions, Solid State Ionics. 148 (2002) 405–416. https://doi.org/10.1016/S0167-2738(02)00080-2.

[6] Y. Takeda, O. Yamamoto, N. Imanishi, Lithium Dendrite Formation on a Lithium Metal Anode from Liquid, Polymer and Solid Electrolytes, Electrochemistry. 84 (2016) 210–218. https://doi.org/10.5796/electrochemistry.84.210.
[7] L. Frenck, G.K. Sethi, J.A. Maslyn, N.P. Balsara, Factors That Control the Formation of Dendrites and Other Morphologies on Lithium Metal Anodes, Frontiers in Energy Research. 7 (2019) 115. https://doi.org/10.3389/fenrg.2019.00115.
[8] D.T. Hallinan, I. Villaluenga, N.P. Balsara, Polymer and composite electrolytes, MRS Bulletin. 43 (2018) 775–781. https://doi.org/10.1557/mrs.2018.212.
[9] E.A. Hogge, M.B. Kraichman, The Limiting Current on a Rotating Disc Electrode in Potassium Iodide-Potassium Triiodide Solutions, Journal of the American Chemical Society. 76 (1954) 1431–1433. https://doi.org/10.1021/ja01634a088.
[10] C.W. Tobias, M. Eisenberg, C.R. Wilke, Diffusion and Convection in Electrolysis—A Theoretical Review, Journal of The Electrochemical Society. 99 (1952) 359C-365C. https://doi.org/10.1149/1.2779636.
[11] H.J.S. Sand, On the concentration at the electrodes in a solution, with special reference to the liberation of hydrogen by electrolysis of a mixture of copper sulphate and sulphuric acid, Proceedings of the Physical Society of London. 17 (1899) 496–534. https://doi.org/10.1088/1478-7814/17/1/332.
[12] Y. Choo, D.M. Halat, I. Villaluenga, K. Timachova, N.P. Balsara, Diffusion and migration in polymer electrolytes, Progress in Polymer Science. 103 (2020) 101220. https://doi.org/10.1016/j.progpolymsci.2020.101220.
[13] J. Evans, C.A. Vincent, P.G. Bruce, Electrochemical measurement of transference numbers in polymer electrolytes, Polymer. 28 (1987) 2324–2328. https://doi.org/10.1016/0032-3861(87)90394-6.
[14] P.G. Bruce, J. Evans, C.A. Vincent, Conductivity and transference number measurements on polymer electrolytes, Solid State Ionics. 28–30 (1988) 918–922. https://doi.org/10.1016/0167-2738(88)90304-9.
[15] P.G. Bruce, F.M. Gray, Polymer Electrolytes II: Physical Principles, in: P.G. Bruce (Ed.), Solid State Electrochemistry, Cambridge University Press, 1995: pp. 157–158. https://doi.org/10.1017/CBO9780511524790.
[16] M.D. Galluzzo, J.A. Maslyn, D.B. Shah, N.P. Balsara, Ohm's law for ion conduction in lithium and beyond-lithium battery electrolytes, The Journal of Chemical Physics. 151 (2019) 020901. https://doi.org/10.1063/1.5109684.
[17] D.B. Shah, H.K. Kim, H.Q. Nguyen, V. Srinivasan, N.P. Balsara, Comparing Measurements of Limiting Current of Electrolytes with Theoretical Predictions up to the Solubility Limit, The Journal of Physical Chemistry C. 123 (2019) 23872–23881. https://doi.org/10.1021/acs.jpcc.9b07121.
[18] C.O. Laoire, E. Plichta, M. Hendrickson, S. Mukerjee, K.M. Abraham, Electrochemical studies of ferrocene in a lithium ion conducting organic carbonate electrolyte, Electrochimica Acta. 54 (2009) 6560–6564. https://doi.org/10.1016/j.electacta.2009.06.041.
[19] S.I. Lee, U.H. Jung, Y.S. Kim, M.H. Kim, D.J. Ahn, H.S. Chun, A study of electrochemical kinetics of lithium ion in organic electrolytes, Korean Journal of Chemical Engineering. 19 (2002) 638–644. https://doi.org/10.1007/BF02699310.
[20] J.W. Park, K. Yoshida, N. Tachikawa, K. Dokko, M. Watanabe, Limiting current density in bis(trifluoromethylsulfonyl)amide-based ionic liquid for lithium batteries, Journal of Power Sources. 196 (2011) 2264–2268. https://doi.org/10.1016/j.jpowsour.2010.09.067.

[21] W.R. Hudson, Block Copolymer Electrolytes for Lithium Batteries, University of California, Berkeley, 2011.
[22] J.A. Maslyn, L. Frenck, V.D. Veeraraghavan, A. Müller, A.S. Ho, N. Marwaha, W.S. Loo, D.Y. Parkinson, A.M. Minor, N.P. Balsara, Limiting Current in Nanostructured Block Copolymer Electrolytes, Macromolecules. 54 (2021) 4010–4022. https://doi.org/10.1021/acs.macromol.1c00425.
[23] D.A. Gribble, L. Frenck, D.B. Shah, J.A. Maslyn, W.S. Loo, K.I.S. Mongcopa, D.M. Pesko, N.P. Balsara, Comparing Experimental Measurements of Limiting Current in Polymer Electrolytes with Theoretical Predictions, Journal of the Electrochemical Society. 166 (2019) A3228-3234. https://doi.org/10.1149/2.0391914jes.
[24] N.P. Balsara, J. Newman, E. Storage, L. Berkeley, Relationship between Steady-State Current in Symmetric Cells and Transference Number of Electrolytes Comprising Univalent and Multivalent Ions, 162 (2015) 2720–2722. https://doi.org/10.1149/2.0651514jes.
[25] D.M. Pesko, Z. Feng, S. Sawhney, J. Newman, V. Srinivasan, N.P. Balsara, Comparing Cycling Characteristics of Symmetric Lithium-Polymer-Lithium Cells with Theoretical Predictions, Journal of The Electrochemical Society. 165 (2018) A3186–A3194. https://doi.org/10.1149/2.0921813jes.
[25] J. Newman, N. P. Balsara, Electrochemical Systems, 4th Edition | Wiley.
[27] L. Frenck, V.D. Veeraraghavan, J.A. Maslyn, A. Müller, A.S. Ho, W.S. Loo, A.M. Minor, N.P. Balsara, Effect of salt concentration profiles on protrusion growth in lithium-polymer-lithium cells, Solid State Ionics. 358 (2020) 115517. https://doi.org/10.1016/j.ssi.2020.115517.
[28] M. Singh, O. Odusanya, G.M. Wilmes, H.B. Eitouni, E.D. Gomez, A.J. Patel, V.L. Chen, M.J. Park, P. Fragouli, H. Iatrou, N. Hadjichristidis, D. Cookson, N.P. Balsara, Effect of Molecular Weight on the Mechanical and Electrical Properties of Block Copolymer Electrolytes, Macromolecules. 40 (2007) 4578–4585. https://doi.org/10.1021/ma0629541.
[29] R.P. Quirk, J. Kim, C. Kausch, M. Chun, Butyllithium-initiated anionic synthesis of well-defined poly(styrene-block-ethylene oxide) block copolymers with potassium salt additives, Polymer International. 39 (1996) 3–10. https://doi.org/10.1002/(SICI)1097-0126(199601)39:1<3::AID-PI436>3.0.CO;2-O.
[30] N. Hadjichristidis, M. Pitsikalis, S. Pispas, H. Iatrou, Polymers with Complex Architecture by Living Anionic Polymerization, Chem. Rev. 101 (2001) 3747–3792. https://doi.org/10.1021/cr9901337.
[31] R. Yuan, A.A. Teran, I. Gurevitch, S.A. Mullin, N.S. Wanakule, N.P. Balsara, Ionic conductivity of low molecular weight block copolymer electrolytes, Macromolecules. 46 (2013) 914–921. https://doi.org/10.1021/ma3024552.
[32] K.J. Harry, D.T. Hallinan, D.Y. Parkinson, A.A. MacDowell, N.P. Balsara, Detection of subsurface structures underneath dendrites formed on cycled lithium metal electrodes, Nature Materials. 13 (2014) 69–73. https://doi.org/10.1038/nmat3793.
[33] K.J. Harry, X. Liao, D.Y. Parkinson, A.M. Minor, N.P. Balsara, Electrochemical Deposition and Stripping Behavior of Lithium Metal across a Rigid Block Copolymer Electrolyte Membrane, J. Electrochem. Soc. 162 (2015) A2699–A2706. https://doi.org/10.1149/2.0321514jes.
[34] J.A. Maslyn, W.S. Loo, K.D. McEntush, H.J. Oh, K.J. Harry, D.Y. Parkinson, N.P. Balsara, Growth of Lithium Dendrites and Globules through a Solid Block Copolymer Electrolyte as

a Function of Current Density, J. Phys. Chem. C. 122 (2018) 26797–26804. https://doi.org/10.1021/acs.jpcc.8b06355.
[35] L. Frenck, J.A. Maslyn, W.S. Loo, D.Y. Parkinson, N.P. Balsara, Impact of Salt Concentration on Nonuniform Lithium Electrodeposition through Rigid Block Copolymer Electrolytes, ACS Appl. Mater. Interfaces. (2019). https://doi.org/10.1021/acsami.9b15606.
[36] P. Arora, Z. (John) Zhang, Battery Separators, Chem. Rev. 104 (2004) 4419–4462. https://doi.org/10.1021/cr020738u.
[37] C. Monroe, J. Newman, Dendrite Growth in Lithium/Polymer Systems A Propagation Model for Liquid Electrolytes under Galvanostatic Conditions, J. Electrochem. Soc. 150 (2003) A1377–A1384. https://doi.org/10.1149/1.1606686.
[38] M. Watanabe, S. Nagano, K. Sanui, N. Ogata, Estimation of Li+ transport number in polymer electrolytes by the combination of complex impedance and potentiostatic polarization measurements, Solid State Ionics. 28–30 (1988) 911–917. https://doi.org/10.1016/0167-2738(88)90303-7.
[39] I. Villaluenga, D.M. Pesko, K. Timachova, Z. Feng, J. Newman, V. Srinivasan, N.P. Balsara, Negative Stefan-Maxwell Diffusion Coefficients and Complete Electrochemical Transport Characterization of Homopolymer and Block Copolymer Electrolytes, J. Electrochem. Soc. 165 (2018) A2766. https://doi.org/10.1149/2.0641811jes.
[40] C. Cao, Y. Li, Y. Feng, C. Peng, Z. Li, W. Feng, A solid-state single-ion polymer electrolyte with ultrahigh ionic conductivity for dendrite-free lithium metal batteries, Energy Storage Materials. 19 (2019) 401–407. https://doi.org/10.1016/j.ensm.2019.03.004.
[41] R. Bouchet, S. Maria, R. Meziane, A. Aboulaich, L. Lienafa, J.-P. Bonnet, T.N.T. Phan, D. Bertin, D. Gigmes, D. Devaux, R. Denoyel, M. Armand, Single-ion BAB triblock copolymers as highly efficient electrolytes for lithium-metal batteries, Nature Materials. 12 (2013) 452–457. https://doi.org/10.1038/nmat3602.
[42] G.M. Stone, S.A. Mullin, A.A. Teran, D.T. Hallinan, A.M. Minor, A. Hexemer, N.P. Balsara, Resolution of the Modulus versus Adhesion Dilemma in Solid Polymer Electrolytes for Rechargeable Lithium Metal Batteries, J. Electrochem. Soc. 159 (2012) A222–A227. https://doi.org/10.1149/2.030203jes.
[43] L. Fan, S. Wei, S. Li, Q. Li, Y. Lu, Recent Progress of the Solid-State Electrolytes for High-Energy Metal-Based Batteries, Advanced Energy Materials. 8 (2018) 1702657. https://doi.org/10.1002/aenm.201702657.
[44] D. Devaux, K.J. Harry, D.Y. Parkinson, R. Yuan, D.T. Hallinan, A.A. MacDowell, N.P. Balsara, Failure Mode of Lithium Metal Batteries with a Block Copolymer Electrolyte Analyzed by X-Ray Microtomography, J. Electrochem. Soc. 162 (2015) A1301–A1309. https://doi.org/10.1149/2.0721507jes.

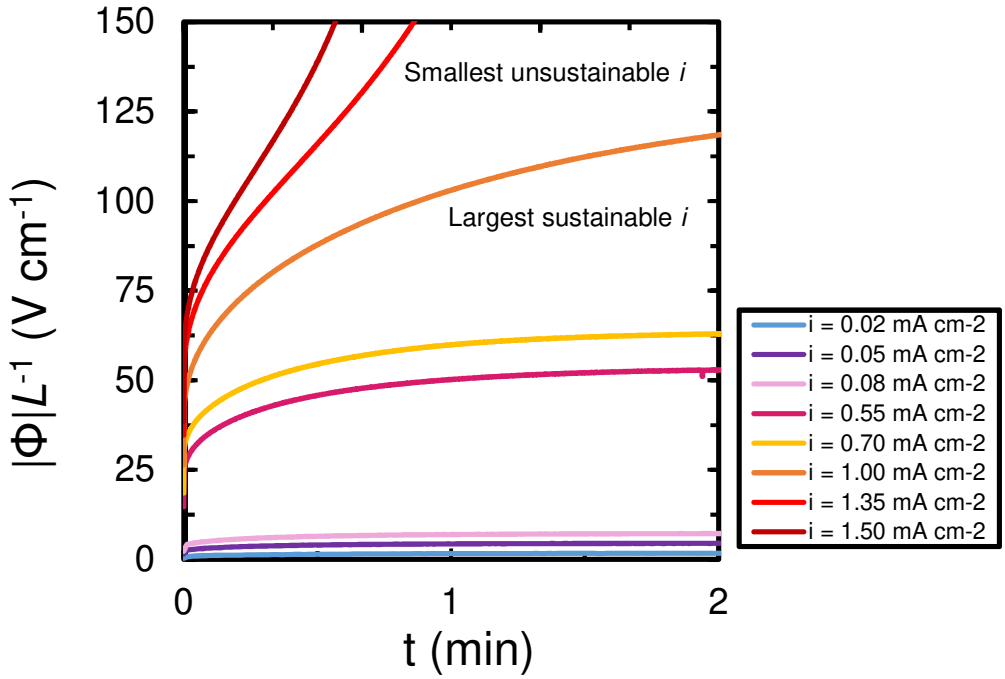

Figure 1. Absolute value of the potential drop across the electrolyte normalized by the thickness, $|\Phi|L^{-1}$, as a function of time for different applied current densities. The measured potential is corrected to account for the potential drop due to interfacial impedances at the electrode/electrolyte interfaces[23,25]. The current density was increased in steps as shown. All data were obtained for one cell with r_{av} = 0.085, and L = 43 μm at 90 °C. Similar data were obtained for all other r_{av} values.

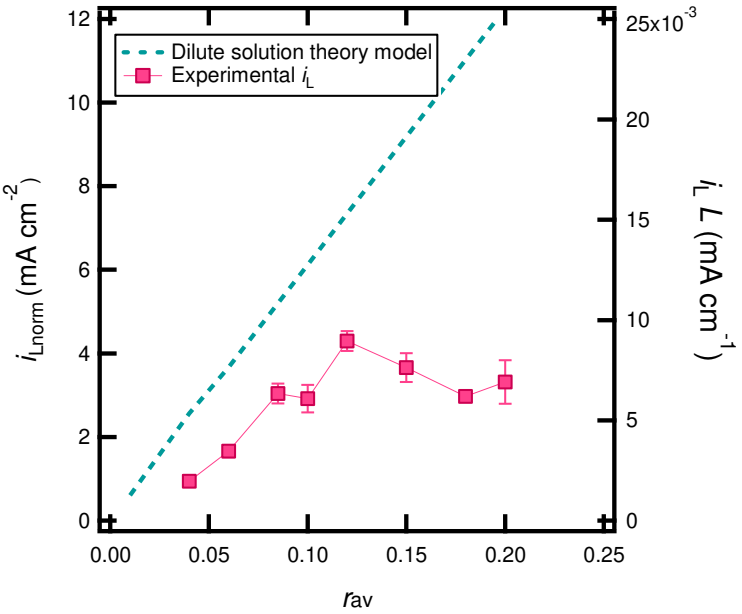

Figure 2. Experimental limiting current density, square pink markers, and predicted limiting current density from dilute solution theory using Eq 2, turquoise dashed line, plotted as a function of salt concentration, r_{av}. On the left y-axis, we show the limiting current density for an electrolyte of 20 µm thickness, i_{Lnorm}, calculated using Eq 1. On the right y-axis we show the limiting current density, i_L, multiplied by the thickness, L. Markers show the experimentally measured limiting current density for an average of 4 to 6 cells. Error bars show the standard deviation of the measured data.

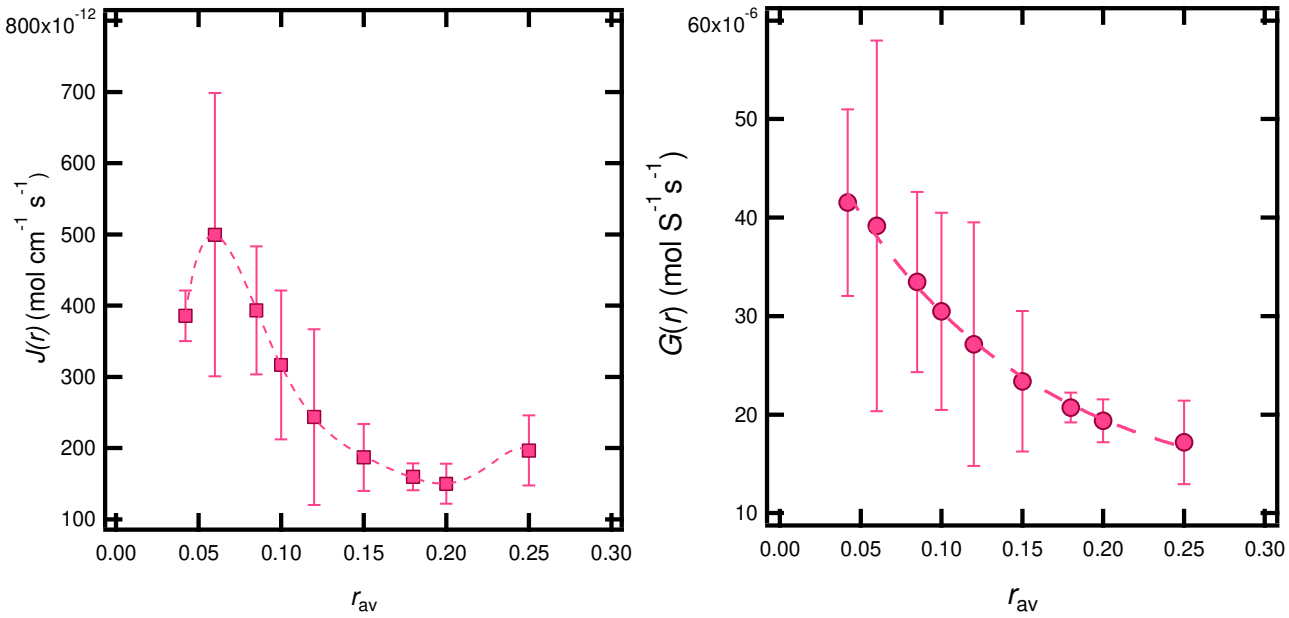

Figure 3. Concentration-dependent functions (a) $J(r)$ and (b) $G(r)$ versus salt concentration r_{av} at 90°C as defined in Eq 3 and Eq 5. The pink dashed curves show the polynomial and double exponential fits for (a) and (b) respectivel,y as defined in Eq 6 and Eq 7; while the markers show the calculated transport coefficients. Error bars represent standard deviations. Panel (a) was published in ref [27] and reproduced with permission.

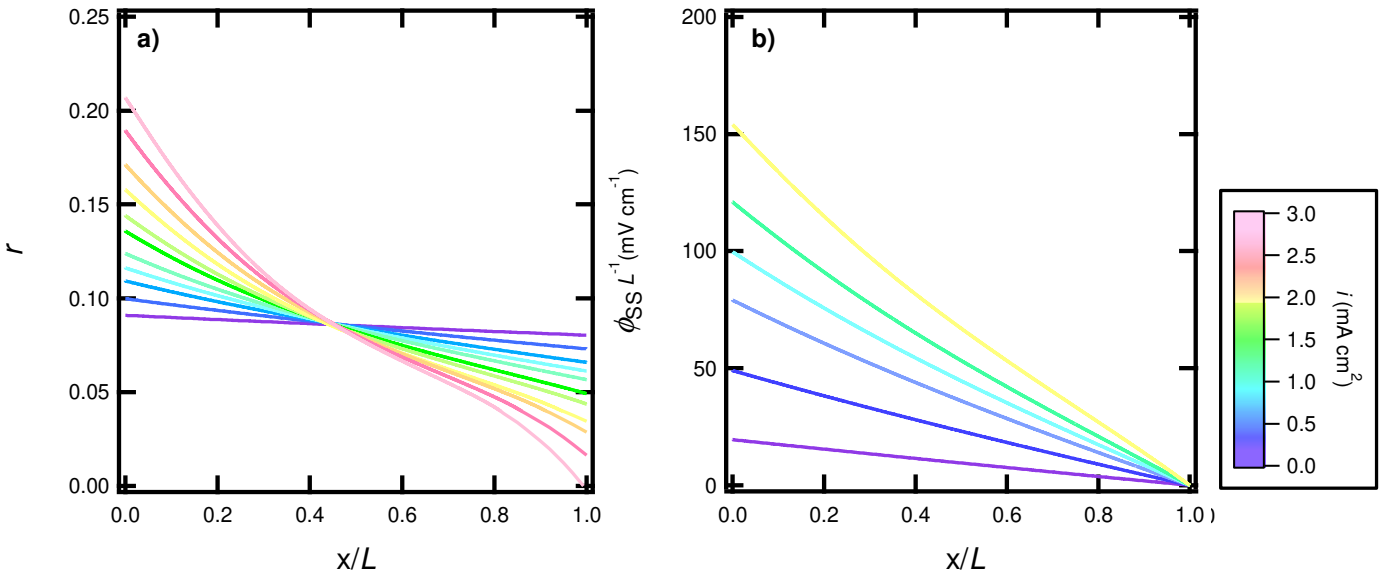

Figure 4. (a) Salt concentration, r, as a function of position x/L in the cell at specified current densities calculated using Eq 3. (b) Steady-state electric potential normalized by thickness, $\Phi_{SS} L^{-1}$ as a function of position x/L at the same current densities calculated using Eq 5. Numerical problems preclude the calculation of potential profiles as the limiting current is approached. Calculations were conducted for a cell with L = 20 µm containing an electrolyte with r_{av} = 0.085 at 90 °C. The cathode side is represented at x/L =1, while the anode side is represented at x/L = 0. When r reaches 0 at x/L = 1 the limiting current density is reached.

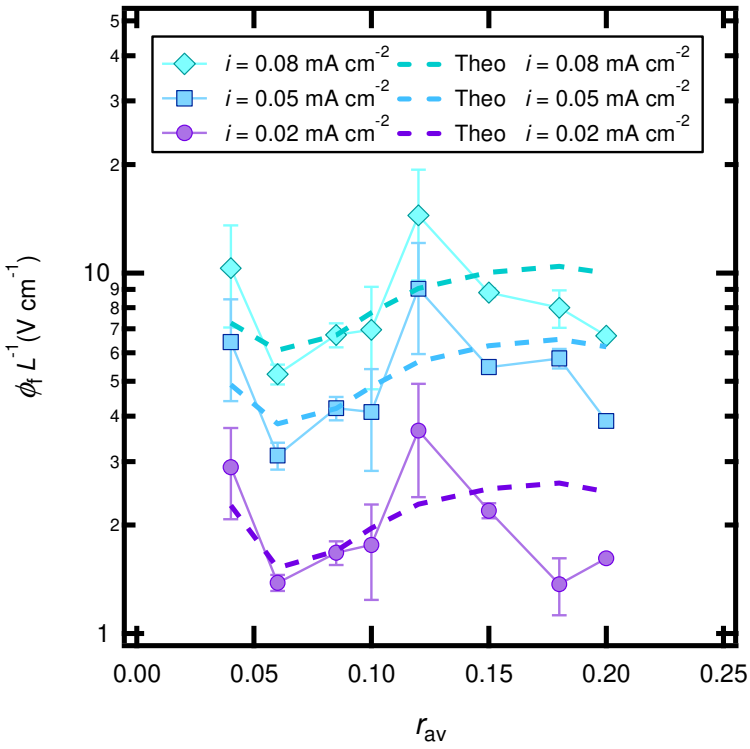

Figure 5. Comparison of experimentally measured steady-state electric potential normalized by thickness, $\Phi_{f,}\ L^{-1}$ (markers) and predicted steady-state potential using Eq 5 (dashed curves) in electrolytes at i = 0.02, 0.05, and 0.08 mA cm^{-2} at 90ºC for 50µm thick membranes. Error bars represent standard deviations for the measured data.

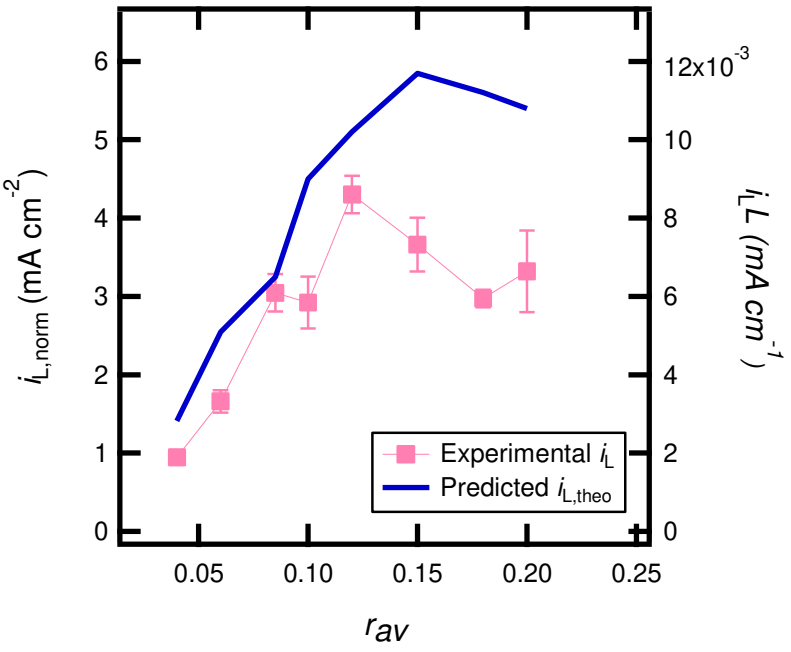

Figure 6. Limiting current density, $i_{L,}$ as a function of salt concentration r_{av} at 90 °C. The solid blue line shows the predicted limiting current density using Eq 3. On the left y-axis, we show the limiting current density for an electrolyte of 20 µm thickness, i_{Lnorm}, calculated using Eq 1. On the right y-axis we show the limiting current density, i_L, multiplied by the thickness, L.

Comparing Measurement of Limiting Current in Block Copolymer Electrolytes as a Function of Salt Concentration with Theoretical Predictions

Louise Frenck[a,b], Vijay D. Veeraraghavan[a], Jacqueline A. Maslyn[a,b] Nitash P. Balsara[a,b]

[a]Department of Chemical and Biomolecular Engineering, University of California, Berkeley, California 94720, United States

[b]Materials Sciences Division, Lawrence Berkeley National Laboratory, Berkeley, California 94720, United States

GRAPHICAL ABSTRACT